OPEN ACCESS
IOP Publishing

Letters
Journal of Physics: Condensed Matter

J. Phys.: Condens. Matter **37** (2025) 10LT01 (5pp)
https://doi.org/10.1088/1361-648X/ada338

Letter

Chiral effects at the metal center in Fe(III) spin crossover coordination salts

M Zaid Zaz[1], Wai Kiat Chin[1], Gauthami Viswan[1], Arjun Subedi[1], Esha Mishra[1,2], Kayleigh A McElveen[3], Binny Tamang[3], David Shapiro[4], Alpha T N'Diaye[4], Rebecca Y Lai[3] and Peter A Dowben[1,*]

[1] Department of Physics and Astronomy, Jorgensen Hall, University of Nebraska-Lincoln, Lincoln, NE 68588-0299, United States of America
[2] Department of Physics, Berry College, 2277 Martha Berry Hwy. NW., Mount Berry, GA 30149, United States of America
[3] Department of Chemistry, Hamilton Hall, University of Nebraska-Lincoln, Lincoln, NE 68588-0304, United States of America
[4] Advanced Light Source, Lawrence Berkeley National Laboratory, Berkeley, CA 94720, United States of America

E-mail: pdowben@unl.edu

Received 9 October 2024, revised 6 December 2024
Accepted for publication 24 December 2024
Published 6 January 2025

Abstract

Evidence of chirality was observed at the Fe metal center in Fe(III) spin crossover coordination salts $[Fe(qsal)_2][Ni(dmit)_2]$ and $[Fe(qsal)_2](TCNQ)_2$ from x-ray absorption (XAS) spectroscopy at the Fe $2p_{3/2}$ core threshold. Based on the circularly polarized XAS data, the x-ray natural circular dichroism for $[Fe(qsal)_2][Ni(dmit)_2]$ and $[Fe(qsal)_2](TCNQ)_2$ is far stronger than seen for $[Fe(qsal)_2]Cl$ suggesting this natural circular dichroism signature is a ligand effect rather than a result of just a loss of octahedral symmetry on the Fe core. The larger the chiral effects in the Fe 2p core to bound XAS, the greater the perturbation of the Fe $2p_{3/2}$ to $2p_{1/2}$ spin–orbit splitting seen in the XAS spectra.

Supplementary material for this article is available online

Keywords: chirality, spin crossover, dichroism

1. Introduction

Chiral behavior has been observed in several spin crossover molecular complexes [1–18] and is generally expected. Chirality in spin crossover systems is often a result of the loss of inversion symmetry, due to the presence of asymmetric ligands. Chirality can also arise due to distorted octahedral coordination resulting from bulky functional groups attached to the ligands or due to the presence of bulky counterions [10, 14, 19–21] or, in principle, the result of the molecular packing. Yet demonstrations of chirality in visible [1–10] and infra-red [8] spectra do little to address the effect of chirality on the metal center weighted molecular orbitals. So, while chirality is common, we ask here whether the chirality from molecular packing and ligand choice influence the octahedrally coordinated iron. X-ray circular dichroism

* Author to whom any correspondence should be addressed.

(XCD) or x-ray natural circular dichroism (XNCD) has been observed for both metal centered molecular complexes [22], and organic systems, typically containing a somewhat larger Z atom, like Cl in chlorophenylethanol or chlorohexahelicene [23]. This XCD or XNCD is distinct from x-ray magnetic circular dichroism (XMCD), as a magnetic moment is not required for XCD/XNCD, just the loss of inversion symmetry [24].

In this paper, we present evidence of chirality in Fe(III) spin crossover coordination salts, namely $[Fe(qsal)_2][Ni(dmit)_2]$, $[Fe(qsal)_2](TCNQ)_2$ where, (qsalH = N-(8-quinolylsalicylaldimine), ($dmit_2-$ = 1,3-dithiol-2-thione-4,5-dithiolato) and (TCNQ = 7,7,8,8-tetracyanoquinodimethane) from spatially resolved x-ray absorption (XAS) spectroscopy, using circularly polarized x-rays. These chiral salts are similar to spin crossover chiral salt complexes that feature large conductance, where $[FeIII(qsal)_2][Ni(dmit)]_2]_3.CH_3CN.H_2O$ has a resistance less than 1 ohm·cm [25], as does $[Fe(III)(3\text{-}OMe\text{-}sal_2trien)][Ni(dmit)_2]$ [26] and $[Fe(III)(sal_2trien)](TCNQ)_2{\cdot}CH_3OH$ [27], while $[Fe(sal_2trien][Ni(dmit)_2]_3$ has a resistance less than 3 Ohm·cm [28], all when in the high spin state at elevated temperatures. These low resistivities are atypical of spin crossover complexes that have no counter ion [29–31], although a counter ion like TCNQ does not ensure this exceptional conductivity [31–34].

2. Experimental

The Fe(III) coordination complex, $[Fe(qsal)_2]Cl$ where (qsalH = N-(8-quinolyl)salicylaldimine), was synthesized in accordance with a protocol reported elsewhere [35]. The procedure for the synthesis of $[Fe(qsal)_2](TCNQ)_2$ followed the procedure for the synthesis of $[Fe(qsal)_2]Cl$, followed by a process detailed elsewhere [27, 34]. $[Fe(qsal)_2][Ni(dmit)_2]$ was also synthesized according to a protocol reported earlier [36]. The Fe to Ni ratio for $[Fe(qsal)_2][Ni(dmit)_2]$ was confirmed by x-ray diffraction and energy dispersive analysis of emitted x-rays (EDAX). While the Fe to Ni ratio is 1:1 from EDAX, consistent the molecular stoichiometry of $[Fe(qsal)_2][Ni(dmit)_2]$, x-ray photoemission (XPS) studies, from the Fe and Ni 2p core levels, indicate that the Fe to Ni ratio is 1:2. This suggests that the surface terminates in $Ni(dmit)_2$, as discussed elsewhere [37]. Consistent with a $Ni(dmit)_2$ surface termination, the surface has a strong surface to bulk core level shift in the Ni 2p core level XPS spectra, resulting from final state effects [37].

The magnetometry measurements of the DC magnetic susceptibility times temperature were carried out in DynaCool SQUID magnetometer from Quantum Design at the Nebraska Center for Materials and Nanoscience. Magnetometry measurements (figure 1) performed on $[Fe(qsal)_2]X$, $X = Ni(dmit)_2$, Cl, or $(TCNQ)_2$, match well with what is reported in the literature on $[Fe(qsal)_2]Cl$ [35] and $[Fe(qsal)_2][Ni(dmit)_2]$ [25, 36]. The magnetometry of $[Fe(qsal)_2](TCNQ)_2$ reveals a gradual spin transition with increasing temperature much like $[Fe(qsal)_2][Ni(dmit)_2]$ and indicates that at room temperature, these three Fe(III) complexes are in the high spin state or nearly so.

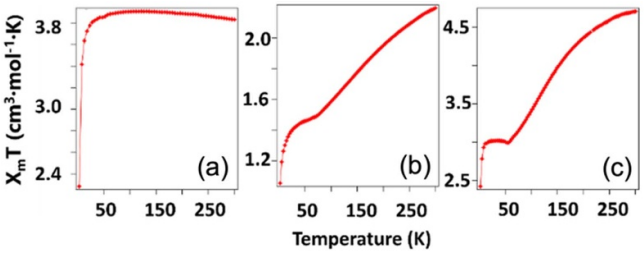

Figure 1. The product of molar magnetic susceptibility and temperature of: (a) $[Fe(qsal)_2]Cl$, (b) $[Fe(qsal)_2][Ni(dmit)_2]$, (c) $[Fe(qsal)_2](TCNQ)_2$, plotted against temperature.

Spatially resolved XAS spectroscopy experiments, using left and right circularly polarized light, were performed on the COSMIC beamline (Beamline 7.0.1.2) at the Advanced light source in Lawrence Berkeley National Laboratories. The incident beam was tuned to the Fe L3 edge (Fe $2p_{3/2}$) at 707 eV, using a small spot size (50 nm) to be able to perform the XAS, with circularly polarized x-rays in the transmission mode, on a single $[Fe(qsal)_2]X$ chiral crystallite domain, X = $Ni(dmit)_2$, Cl, or $(TCNQ)_2$. This resembles the spatially resolved element-specific XNCD studies of multiferroic crystals [38]. The relative local Ni and Fe moments were investigated with XAS and XMCD spectroscopies at beamline 6.3.1 (Advanced Light Source, Berkeley, CA), using total electron yield and circularly polarized x-rays with an estimated degree of polarization of 0.66. The XMCD spectra were obtained with an applied field of 1.8 T. The inverse photoemission (IPES) experiments were acquired in the isochromatic mode with a commercial high resolution electron gun (Kimball Physics) combined with channeltron-based photon detector (OmniVac).

3. X-ray natural circular dichroism

Figure 2 shows the XAS spectra at the Fe L2 ($2p_{1/2}$) and L3 ($2p_{3/2}$) edges, for single chiral domains of $[Fe(qsal)_2]X$, X = $Ni(dmit)_2$, Cl, and $(TCNQ)_2$, obtained using right and left circularly polarized x-ray radiation in the absence of any applied external field. For $[Fe(qsal)_2](TCNQ)_2$, right circularly polarized x-rays excite the Fe $2p_{3/2}$ core electrons to populate both the unoccupied t_{2g} and e_g states, resulting in two distinct peaks at the Fe L3 ($2p_{3/2}$) edge, while as for left circularly polarized x-rays core excitation favors the population of the unoccupied t_{2g} states at lower photon energies. This indicates the existence of x-ray circular polarization dependent selection rules. Similar XNCD behavior is observed for $[Fe(qsal)_2][Ni(dmit)_2]$, though a little less dramatic. For $[Fe(qsal)_2]Cl$, however, we see that the XAS spectra for both right and left circularly polarized x-rays are similar, although still not identical.

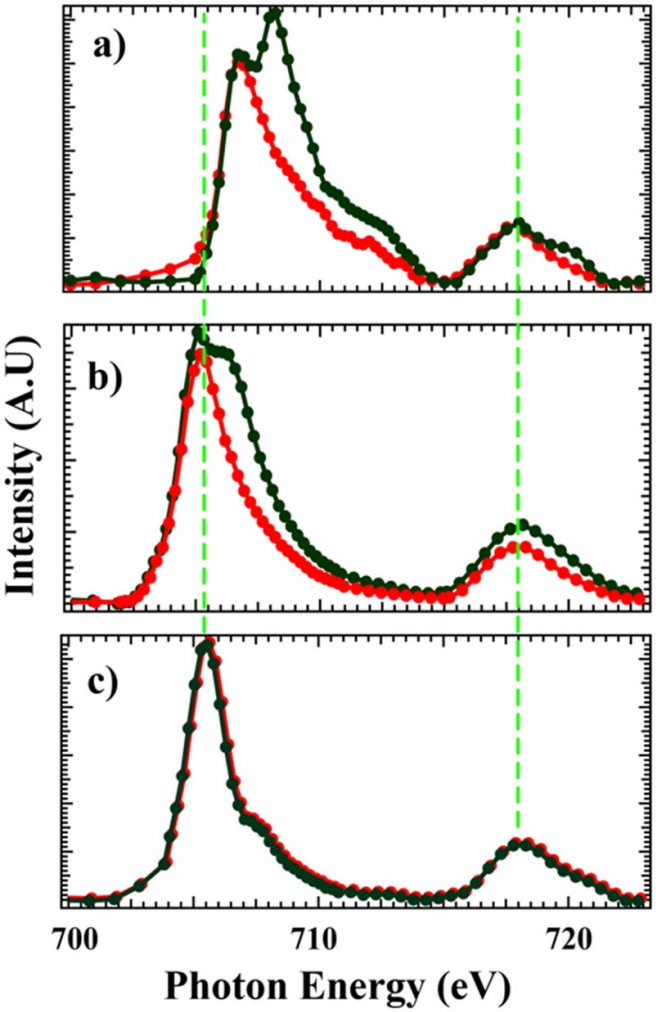

Figure 2. The Fe L2 ($2p_{1/2}$) and L3 ($2p_{3/2}$) edge x-ray absorption spectra of (a) $[Fe(qsal)_2](TCNQ)_2$, (b) $[Fe(qsal)_2][Ni(dmit)_2]$, (c) $[Fe(qsal)_2]Cl$, obtained using right circularly polarized (black) and left circularly polarized (red) x-ray radiation.

4. X-ray magnetic circular dichroism

Figure 3 shows that there is a small XMCD signal (4%) at the Fe 2p core edges, for $[Fe(qsal)_2][Ni(dmit)_2]$, under a 1.8 T applied magnetic field. This XMCD signal is most evident at the Fe $2p_{3/2}$ core edge, indicative that the Fe spin moment dominates. The Fe moment from the $Fe(qsal)_2$ moiety is anti-parallel with the moment from the $Ni(dmit)_2$ moiety, as the XMCD response is opposite in sign with respect to the applied magnetic field. This contrast between the XMCD at the Fe $2p_{3/2}$ (figure 3) and at the Ni $2p_{3/2}$ core (figure 4) make a compelling case for antiferromagnetic alignment of Fe and Ni in $[Fe(qsal)_2][Ni(dmit)_2]$.

It is significant that the $[Fe(qsal)_2][Ni(dmit)_2]$ XMCD spectra of figure 3 do not resemble the XNCD of figure 2. So, not only is the Ni of $[Fe(qsal)_2][Ni(dmit)_2]$ antiferromagnetically coupled to the Fe metal center, but the Fe $2p_{3/2}$ x-ray chiral dichroism signal of $[Fe(qsal)_2]Ni(dmit)_2]$, results from different selection rules than Fe $2p_{3/2}$ XMCD.

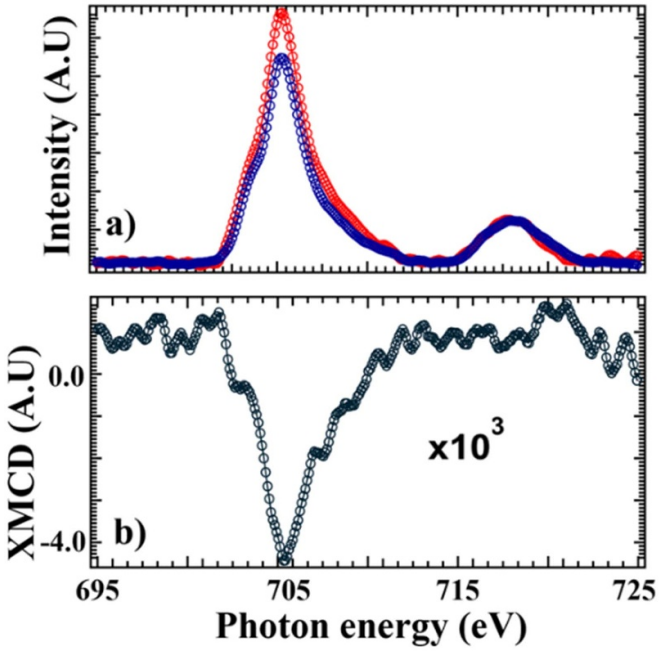

Figure 3. (a) The Fe L2 ($2p_{1/2}$) and L3 ($2p_{3/2}$) x-ray absorption spectra for $[Fe(qsal)_2][Ni(dmit)_2]$ in a 1.8 T applied magnetic field parallel to the sample normal (red), anti-parallel to the sample normal (blue), (b) the XMCD spectrum is extracted from the magnetic field dependent x-ray absorption spectra, seen in (a).

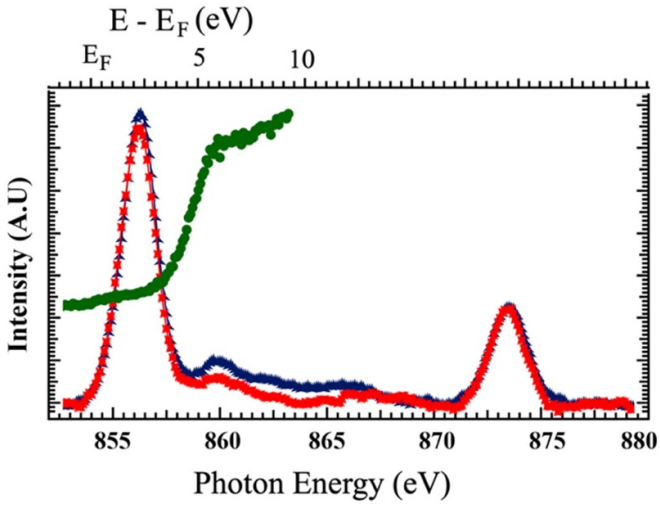

Figure 4. The Ni L2 ($2p_{1/2}$) and L3 ($2p_{3/2}$) x-ray absoption spectra for $[Fe(qsal)_2][Ni(dmit)_2]$ in a 1.8 T applied magnetic field parallel to the sample normal (red), anti-parallel o the sample normal (blue). Overlaid upon the x-ray abosprtion spectra is the inverse photoemission spectru for $[Fe(qsal)_2][Ni(dmit)_2]$, plotted in green, indicating the unoccupied density of states above the Fermi level (chemical potential) E_F, as indicated by the scale bar at the top.

Because the largest differences seen with oppositely applied magnetic field in the XAS, occur at photon energies well above Ni $2p_{3/2}$ (figure 4), the origin of the Ni $2p_{3/2}$ XMCD signal cannot simply be the Ni metal center by itself. Because IPES is very surface sensitive and because the surface of the

$[Fe(qsal)_2][Ni(dmit)_2]$ thin film terminates in $Ni(dmit)_2$ [37], as determined by XPS, the IPES is representative mostly of the 1,3-dithiol-2-thione-4,5-dithiolato ligand (dmit) unoccupied density of states. This unoccupied ligand (dmit) density of states overlaps the region where the XMCD signal is the greatest, at photon energies well above the Ni $2p_{3/2}$ core threshold. Thus, a substantial fraction of the moment on the $Ni(dmit)_2$ moiety appears to reside on the ligand itself and implies that antiferromagnetic coupling between the Ni and Fe is mediated by the ligand.

5. Discussion

The light circular polarization dependence of the XAS of $[Fe(qsal)_2](TCNQ)_2$ and $[Fe(qsal)_2][Ni(dmit)_2]$ (figures 2(a) and (b)) can either be a result of XMCD or x-ray chiral effects, i.e. XCD or XNCD [24]. As noted above, the x-ray circular dichroism results, of figure 2, were obtained in the absence of an applied magnetic field, and do not resemble the XMCD of figure 3. In fact, the x-ray absorption spectra, taken to create the XMCD spectrum, resembles the sum of the XAS spectra taken as a function of both left and right circular polarization for $[Fe(qsal)_2][Ni(dmit)_2]$ (figure 2(b)), as seen in figure 5(a). The XAS, taken with right circularly polarized light at the Fe $2p_{3/2}$ core, summed over many, randomly oriented, $[Fe(qsal)_2][Ni(dmit)_2]$ crystallites (figure 5(b)) also resembles the XAS spectra of figure 3, as is, in fact, expected. It is noteworthy that these chiral spin crossover thin films possess multiple domains, that is to say that the circular polarization dependence of the x-ray irradiation occurs, for both left and right circularly polarized x-rays, becomes negligible if a large number of domains are included. The XAS differences, as a function of incident x-ray circular polarization, varies in spatially disjoint regions, indicating that chiral crystallite domains of both molecular enantiomers exist.The XAS dependence on light circular polarization, observed at the Fe $2p_{3/2}$ core, seen in figure 2, is thus an x-ray chiral circular dichroism effect implying loss of inversion symmetry, not an XMCD signal resulting from a net magnetic moment [24].

The chiral texture affects the Fe weighted molecular orbitals. Chirality imparts spin–orbit coupling, due to the loss of inversion symmetry. The strong chiral effects, that leads to spin–orbit coupling, that now appears within the Fe $2p_{3/2}$ envelope, appears to affect the Fe $2p_{3/2}$ to $2p_{1/2}$ spin–orbit splitting as the latter is diminished for $[Fe(qsal)_2](TCNQ)_2$ and $[Fe(qsal)_2Ni(dmit)_2$ compared to $[Fe(qsal)_2]Cl$, as seen in figure 2. The XAS Fe $2p_{3/2}$ to Fe $2p_{1/2}$ spin orbit splitting is significantly smaller (approximately 0.6–2.4 eV) for $[Fe(qsal)_2](TCNQ)_2$ that for either $[Fe(qsal)_2][Ni(dmit)_2]$ (approximately 0.6 eV) or $[Fe(qsal)_2]Cl$ (approximately 2.4 eV), as seen in figure 2. The Fe $2p_{3/2}$ to Fe $2p_{1/2}$ spin orbit splitting, seen in XAS for $[Fe(qsal)_2]Cl$ (figure 2(c)), is roughly 12.7 eV, close to the value expect for the Fe 2p core (13 eV). The perturbation to the Fe 2p spin–orbit splitting, seen in XAS for $[Fe(qsal)_2](TCNQ)_2$ (figure 2(a)) and to a much smaller extent for $[Fe(qsal)_2][Ni(dmit)_2]$ is unlikely to be an initial state effect. The initial state spin–orbit splitting of a core level should be dominated by the atomic spin–orbit splitting, which should be insensitive to the ligand field. The fact that the perturbations to the Fe 2p spin–orbit splitting $[Fe(qsal)_2](TCNQ)_2$ (figure 2(a)) and $[Fe(qsal)_2][Ni(dmit)_2]$ are largest in the XAS final state where the chiral effects are greatest is noteworthy, as loss of inversion symmetry does impart spin-orbit coupling.

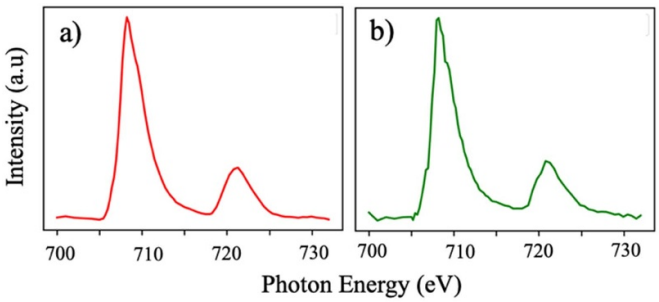

Figure 5. (a) The Fe L2 ($2p_{1/2}$) and L3 ($2p_{3/2}$) x-ray absorption spectrum for $[Fe(qsal)_2][Ni(dmit)_2]$ after summing x-ray absorption spectra taken for both left and right circular polarized x-ray fluence, for a single chiral crystallite, (b) The Fe L2 ($2p_{1/2}$) and L3 ($2p_{3/2}$) x-ray absorption spectrum for a sum of multiple $[Fe(qsal)_2][Ni(dmit)_2]$ randomly oriented crystallites.

6. Conclusion

In summary, we have shown the presence of a strong chiral texture in Fe(III) spin crossover coordination salts with heavy counterions. The Fe core is sufficiently perturbed within a single chiral domain crystallite to result in strong chiral effects at the Fe $2p_{3/2}$ core threshold in circularly polarized light dependent XAS spectroscopy of the Fe(III) spin crossover coordination salts $[Fe(qsal)_2Ni(dmit)_2]$ and $[Fe(qsal)_2][(TCNQ)_2$ but not $[Fe(qsal)_2]Cl$. The absence of significant chiral effects for $[Fe(qsal)_2]Cl$ indicate that inversion symmetry breaking the For metal center alone might not be sufficient to observe chiral effects. In spite of the fact we have measure here the chiral signal of the Fe metal center, the bulky counterions are certainly implicated as contributing to the observed XNCD of the Fe metal center. X-ray chiral effects observed for an individual crystallite domain of $[Fe(qsal)_2][Ni(dmit)_2]$ are distinct from x-ray magnetic dichroism effects and thus constitute an x-ray natural circular dichoism distinct from XMCD. Magnetic dichroism was also observed and indicate that Fe center is antiferromagnetically aligned with Ni in $[Fe(qsal)_2][Ni(dmit)_2]$.

Data availability statement

The raw data files for the data shown in this paper has been made available in the supplementary materials.

Acknowledgment

This work was supported by the National Science Foundation (NSF) through the NSF-DMR-EPM 2317464 (MZZ, WKC, GV, EM and PAD), and EPSCoR RII Track-1: Emergent Quantum Materials and Technologies (EQUATE) (KAM, RL and BT). This research used resources of the Advanced Light Source, which is a DOE Office of Science User Facility under Contract No. DE-AC02-05CH11231.

ORCID iDs

M Zaid Zaz https://orcid.org/0000-0001-7849-4715
Wai Kiat Chin https://orcid.org/0000-0002-1840-0825
Gauthami Viswan https://orcid.org/0000-0002-6241-5426
Arjun Subedi https://orcid.org/0000-0002-7581-8144
Esha Mishra https://orcid.org/0000-0002-8317-9370
Kayleigh A McElveen https://orcid.org/0000-0002-1030-2913
David Shapiro https://orcid.org/0000-0002-4186-6017
Alpha T N'Diaye https://orcid.org/0000-0001-9429-9776
Rebecca Y Lai https://orcid.org/0000-0002-1732-9481
Peter A Dowben https://orcid.org/0000-0002-2198-4710

References

[1] Liu W, Bao X, Mao L-L, Tucek J, Zboril R, Liu J-L, Guo F-S, Ni Z-P and Tong M-L 2014 *Chem. Commun.* **50** 4059–61
[2] Gural'skiy I A, Reshetnikov V A, Szebesczyk A, Gumienna-Kontecka E, Marynin A I, Shylin S I, Ksenofontov V and Fritsky I O 2015 *J. Mater. Chem.* C **3** 4737–41
[3] Sunatsuki Y *et al* 2003 *Angew. Chem.* **115** 1652–6
[4] Sunatsuki Y *et al* 2004 *Inorg. Chem.* **43** 4154–71
[5] Sato T, Iijima S, Kojima M and Matsumoto N 2009 *Chem. Lett.* **38** 178–9
[6] Tian L, Pang C-Y, Zhang F-L, Qin L-F, Gu Z-G and Li Z 2015 *Inorg. Chem. Commun.* **53** 55–59
[7] Kelly C T, Jordan R, Felton S, Müller-Bunz H and Morgan G G 2023 *Chem. Eur. J.* **29** e202300275
[8] Ru J, Yu F, Shi P, Jiao C, Li C, Xiong R, Liu T, Kurmoo M and Zuo J 2017 *Eur. J. Inorg. Chem.* **2017** 3144–9
[9] Suryadevara N *et al* 2021 *Chem. Eur. J.* **27** 15172–80
[10] Kucheriv O I, Oliynyk V V, Zagorodnii V V, Launets V L, Fritsky I O and Gural'skiy I A 2020 Modern magnetic and spintronic materials *NATO Science for Peace and Security Series—B: Physics and Biophysics* ed A Kaidatzis, S Sidorenko, I Vladymyrskyi and D Niarchos (Springer) pp 119–43
[11] Ren D-H, Qiu D, Pang C-Y, Li Z and Gu Z-G 2015 *Chem. Commun.* **51** 788–91
[12] Charytanowicz T, Dziedzic-Kocurek K, Kumar K, Ohkoshi S-I, Chorazy S and Sieklucka B 2023 *Cryst. Growth Des.* **23** 4052–64
[13] Iazzolino A, Hamouda A O, Naim A, Rosa P and Freysz E 2017 *2017 Conf. on Lasers and Electro-Optics Europe & European Quantum Electronics Conf. (Cleo/europe-eqec)* (IEEE) p 338
[14] Qin L-F, Pang C-Y, Han W-K, Zhang F-L, Tian L, Gu Z-G, Ren X and Li Z 2015 *Cryst. Eng. Commun.* **17** 7956–63
[15] Zhao X-H, Deng Y-F, Huang J-Q, Liu M and Zhang Y-Z 2024 *Inorg. Chem. Front.* **11** 808–16
[16] Ma T-T, Sun X-P, Yao Z-S and Tao J 2020 *Inorg. Chem. Front.* **7** 1196–204
[17] Bartual-Murgui C, Piñeiro-López L, Valverde-Muñoz F J, Muñoz M C, Seredyuk M and Real J A 2017 *Inorg. Chem.* **56** 13535–46
[18] Regueiro A, García-López V, Forment-Aliaga A and Clemente-León M 2024 *Dalton Trans.* **53** 10637–43
[19] Ortega-Villar N, Muñoz M and Real J 2016 *Magnetochemistry* **2** 16
[20] Shatruk M, Phan H, Chrisostomo B A and Suleimenova A 2015 *Coord. Chem. Rev.* **289–290** 62–73
[21] Ekanayaka T K *et al* 2023 *Mater. Chem. Phys.* **296** 127276
[22] Peacock R D and Stewart B 2001 *J. Phys. Chem.* B **105** 351–60
[23] Zhang Y, Rouxel J R, Autschbach J, Govind N and Mukamel S 2017 *Chem. Sci.* **8** 5969
[24] Bouldi N *et al* 2017 *Phys. Rev.* B **96** 085123
[25] Takahashi K, Cui H-B, Okano Y, Kobayashi H, Einaga Y and Sato O 2006 *Inorg. Chem.* **45** 5739–41
[26] Shvachko Y N, Spitsyna N G, Starichenko D V, Zverev V N, Zorina L V, Simonov S V, Blagov M A and Yagubskii E B 2020 *Molecules* **25** 4922
[27] Shvachko Y, Starichenko D, Korolyov A, Kotov A, Buravov L, Zverev V, Simonov S, Zorina L and Yagubskii E 2017 *Magnetochemistry* **3** 9
[28] Faulmann C, Dorbes S, Real J A and Valade L 2007 *J. Low Temp. Phys.* **142** 265–70
[29] Zaz M Z, Ekanayaka T K, Cheng R and Dowben P A 2023 *Magnetochemistry* **9** 223
[30] Rubio-Giménez V, Tatay S and Martí-Gastaldo C 2020 *Chem. Soc. Rev.* **49** 5601–38
[31] Wang M, Li Z-Y, Ishikawa R and Yamashita M 2021 *Coord. Chem. Rev.* **435** 213819
[32] Phan H, Benjamin S M, Steven E, Brooks J S and Shatruk M 2015 *Angew. Chem.* **54** 823–7
[33] Pukacki W and Graja A 1988 *Synth. Met.* **24** 137–43
[34] Shvachko Y N *et al* 2016 *Inorg. Chem.* **55** 9121–30
[35] Dickinson R C, Baker W A and Collins R L 1977 *J. Inorg. Nucl. Chem.* **39** 1531–3
[36] Faulmann C, Dorbes S, Lampert S, Jacob K, Garreau de Bonneval B, Molnár G, Bousseksou A, Real J A and Valade L 2007 *Inorganica Chim. Acta* **360** 3870–8
[37] Zaz M Z, Tamang B, McElveen K A, Mishra E, Viswan G, Chin W K, Subedi A, N'Daiye A T, Lai R Y and Dowben P A 2024 The surface termination of a Fe (III) spin crossover molecular salt *J. Phys.: Condens. Matter* submitted to (arXiv:2408.07138)
[38] Platunov M S, Gudim I A, Ovchinnikova E N, Kozlovskaya K A, Wilhelm F, Rogalev A, Hen A, Ivanov V Y, Mukhin A A and Dmitrienko V E 2021 *Crystals* **11** 531